SCIENCE CHINA
Earth Sciences

•RESEARCH PAPER•

January 2020 Vol.63 No.1: 37–51
https://doi.org/10.1007/s11430-019-9391-1

Climatology of tropical cyclone tornadoes in China from 2006 to 2018

Lanqiang BAI[1,2,3], Zhiyong MENG[2*], Kenta SUEKI[4], Guixing CHEN[1,3] & Ruilin ZHOU[2]

[1] *School of Atmospheric Sciences, and Guangdong Province Key Laboratory for Climate Change and Natural Disaster Studies, Sun Yat-sen University, Guangzhou 510275, China;*
[2] *Laboratory for Climate and Ocean-Atmosphere Studies, Department of Atmospheric and Oceanic Sciences, School of Physics, Peking University, Beijing 100871, China;*
[3] *Southern Marine Science and Engineering Guangdong Laboratory (Zhuhai), Zhuhai 519000, China;*
[4] *RIKEN Center for Computational Science, Kobe 650-0047, Japan*

Received March 12, 2019; revised June 14, 2019; accepted July 11, 2019; published online September 12, 2019

Abstract We surveyed the occurrence of tropical cyclone (TC) tornadoes in China from 2006 to 2018. There were 64 cataloged TC tornadoes, with an average of five per year. About one-third of the landfalling TCs in China were tornadic. Consistent with previous studies, TC tornadoes preferentially formed in the afternoon shortly before and within about 36 h after landfall of the TCs. These tornadoes mainly occurred in coastal areas with relatively flat terrains. The maximum number of TC tornadoes occurred in Jiangsu and Guangdong provinces. Most of the TC tornadoes were spawned within 500 km of the TC center. Two notable characteristics were found: (1) TC tornadoes in China mainly occurred in the northeast quadrant (Earth-relative coordinates) rather than the right-front quadrant (TC motion-relative coordinates) of the parent TC circulation; and (2) most tornadoes were produced by TCs with a relatively weak intensity (tropical depressions/storms), in contrast with the United States where most tornadoes are associated with stronger TCs. Further analyses showed that TC tornadoes in China tend to be spawned in an environment with large low-level storm relative helicity and large convective available potential energy taking entrainment effects into account. TC tornadoes were particularly active in 2018, with 24 reported tornadoes accounting for 37.5% of the total surveyed samples. The first recorded tornado outbreak in the modern history of China occurred in the envelope of TC Yagi (2018), in which 11 tornadoes were reported in association with significant midlevel intrusions of dry air and the interaction of Yagi with an approaching midlatitude midlevel trough.

Keywords Tornadoes, Tropical cyclones, Historical statistics, China

Citation: Bai L, Meng Z, Sueki K, Chen G, Zhou R. 2020. Climatology of tropical cyclone tornadoes in China from 2006 to 2018. Science China Earth Sciences, 63: 37–51, https://doi.org/10.1007/s11430-019-9391-1

1. Introduction

Landfalling tropical cyclones (TCs) often spawn tornadoes (hereinafter referred to as TC tornadoes), which pose a threat to both human life and property in coastal regions (e.g., Hill et al., 1966; Novlan and Gray, 1974; Gentry, 1983; McCaul Jr, 1991; Edwards, 2012). About 59% of the TCs that hit the United States from 1948 to 1986 (McCaul Jr, 1991) and about 40% of the TCs that made landfall in Japan from 1961 to 1982 (Mitsuta, 1983) produced at least one tornado (Suzuki et al., 2000). The top three producers of TC tornadoes in the United States even spawned >100 tornadoes each (Edwards, 2012). Although TC tornadoes are generally less intense than their midlatitude counterparts (e.g., Novlan and Gray, 1974; McCaul Jr, 1987; Spratt et al., 1997), they cause about 10% of the fatalities and about 0.5% of the damage to

* Corresponding author (email: zymeng@pku.edu.cn)

property attributable to their parent landfalling TCs (Novlan and Gray, 1974).

The database of TC tornadoes has been well established in the United States for decades, which greatly advances the knowledge for the basic characteristics of TC tornadoes and the understanding of tornado threat within the envelope of a landfalling TC. According to statistics from the United States, TC tornadoes can form at any time of day, but the maximum number occurs in the mid- to late afternoon (14:00–17:00 local time) (Schultz and Cecil, 2009). This diurnal variation suggests that solar heating may play an important role in the formation of TC tornadoes, although most of the tornadoes form in a cloudy environment within the TC envelope (McCaul Jr, 1991). There is no distinct relationship between this diurnal variation in the occurrence of TC tornadoes and the time of TC landfall. Most TC tornadoes occur during the day, whereas strong TC tornadoes mainly occur at night (Edwards, 2012). The climatological spatial distribution of TC tornadoes shows that the tornado-favorable region is located in the northeast (Earth-relative coordinates) or right-front (TC motion-relative coordinates) quadrants. More than 80% of tornadoes take place in the northeast quadrant (Schultz and Cecil, 2009). Because the majority of TCs that make landfall have a northward component of translational motion, most TC tornadoes are also located in the right-front quadrant with respect to the TC motion. Over 90% of tornadoes occur in an azimuthal sector between 340° and 120° (where due east is 0°) relative to the TC motion (Schultz and Cecil, 2009). The highest concentration of tornadoes is located from 100 to 500 km in the radial direction from the eye of TC (Edwards, 2012). About 94% of TC tornadoes occur within 400 km of the coast (Schultz and Cecil, 2009). In particular, about 44% of TC tornadoes occur within 50 km of the coast. An understanding of these statistical characteristics is helpful in studying the mechanisms of the formation of TC tornadoes and will help to improve disaster preparedness and mitigation measures for landfalling TCs.

Tornadoes spawned from TCs are an important subset of tornadoes. About 6% of the reported tornadoes in the United States originate within TC envelopes. There were about 73 U.S. TC tornadoes each year from 1955 to 2010 (Edwards, 2012). In Japan, about 20% of tornadoes are associated with TCs (Niino et al., 1997). The annual number of TC tornadoes is five and they mainly occur from the end of August to the end of September. About eight TCs make landfall over China each year (including tropical depressions; calculated using data from 1949 to 2016 from tcdata.typhoon.org.cn; Ying et al., 2014), whereas only about three tropical storms and hurricanes make landfall in the United States annually (Lyons, 2004). However, a systematic analysis of historical TC tornadoes in contiguous China has been missing. Attention of the meteorological bureau and the public has long been paid to the risks from strong winds in or near the TC eyewall, storm surges and flash flooding. The threat from tornadoes within TCs has been greatly underestimated, partly due to the lack of statistics for the historical TC tornadoes (Yao et al., 2019).

Previous studies on TC tornadoes in China have mainly focused on individual case reviews or a regional climate of TC tornadoes. The first documented TC tornado in China occurred on 11 August 1923 near Tianjin (Barbour, 1924). Located in the flat terrain of central eastern China, Jiangsu Province has the highest frequency of tornadoes (Fan and Yu, 2015; Chen et al., 2018) and squall lines (Meng et al., 2013). The deadliest tornado in the past 42 years in China also occurred in Jiangsu Province (Meng et al., 2018). About 20% of the tornado reports in Jiangsu Province are associated with TCs (Zheng et al., 2015). There were 18 and five TC tornadoes recorded in Jiangsu Province during 1962–1984 and 2005–2014, respectively (Shen, 1990; Zheng et al., 2015). Neighboring Jiangsu Province, Shanghai was hit by 23 TC tornadoes during 1962–1971 (Chen and Ding, 1979). The coastal region of southern China is another tornado-prone sector in China (Fan and Yu, 2015; Chen et al., 2018); there are many reports of TC tornadoes from Hainan Province and the Pearl River Delta region of Guangdong Province (e.g., Huang et al., 2014; Zheng et al., 2015; Zheng et al., 2017; Zhao et al., 2017; Bai et al., 2017).

Increasing numbers of high-impact TC tornadoes have come to the attention of the public in China in recent years, especially in 2015 (Bai et al., 2017; Zhao et al., 2017) and 2018. With the increasing online exposure of TC tornadoes, both the general public and meteorologists in China have become more aware of TC tornadoes. Also, it is worth noting that there is a large population within 150 km of the coastline in China, especially in Guangdong Province. TC tornadoes thus may have a huge threat to human lives. This study aims to formulate a basic climatology of TC tornadoes in China using the most comprehensive records from recent decades and to examine the spatial distributions of some key environmental parameters that have been found to be closely related with TC tornadoes in recent studies. In particular, the TC tornadoes that occurred in 2018 were discussed given their high societal impact. By revealing some basic statistics of TC tornadoes in contiguous China, the tornado threat within TC envelopes can be characterized.

2. Data sources and methods

Records on TC tornadoes from 2006 to 2018 were surveyed from various sources, including almost all the existing individual research papers on tornadoes in China, the *Yearbook of Meteorological Disasters in China* (published yearly since 2005 by China Meteorological Press), the *Full Collection of*

Meteorological Disasters in China (published by China Meteorological Press), the database of tornadoes in contiguous China used by Chen et al. (2018), local meteorological agencies and social media. More details about the two book sources can be found in Chen et al. (2018). We defined the study period as 2006–2018 based on the availability of data from Doppler weather radar stations and the fact that the *Yearbook of Meteorological Disasters in China* was first published in 2005. Tornadoes that occur during the day have been increasingly photographed and shared online in the last decade as a result of the popularization of smart phones and digital cameras and increased public awareness. As a consequence, the dataset for tornadoes surveyed from 2006 to 2018 is both stable and relatively complete, with only a small probability that individual TC tornadoes have not been recorded.

The TC best-track data were obtained from the Japan Meteorological Agency (http://agora.ex.nii.ac.jp/digital-typhoon). Based on the Chinese National Standard for the Grade of Tropical Cyclones (GB/T 19201–2006), the intensity scales for TCs used in this study are: tropical depression (TD, 10.8–17.1 m s^{-1}); tropical storm (TS, 17.2–24.4 m s^{-1}); severe tropical storm (STS, 24.5–32.6 m s^{-1}); typhoon (TY, 32.7–41.4 m s^{-1}); severe typhoon (STY, 41.5–50.9 m s^{-1}); and super typhoon (≥51.0 m s^{-1}). Specifically, if a tornado-producing TC only had the intensity of TD during its entire lifespan, then the corresponding tornado was also regarded as a TC tornado. The position of the TC center at the tornado time was estimated by linearly interpolating the Japan Meteorological Agency best-track data.

The tornadoes extracted from various data sources were carefully verified. A TC tornado event was defined as occurring when the tornado was located within 800 km of the center of the parent TC (McCaul Jr, 1991). If a tornado occurred in a distance >800 km but embedded in a TC rainband, it was still regarded as a TC tornado. By reviewing the available data from operational Doppler radar stations, events that did not correspond to a convective storm were rejected. Tornadoes that had no cyclonic rotational signature at the lowest two levels in the radial velocity field were also rejected. It is possible that there was some bias in the reported locations and times of tornado reports. These samples were checked against the radar data within 50 km (1 h) of the reported locations (time). If there was no radar data available, only the tornadoes obtained from research papers or official reports, or with visual evidence, were cataloged.

Events in which the funnel cloud touched the ground several times within a relatively short time were counted as one tornado in consideration of the continuity of the tornado vortex. If a tornado was observed to occur at least 20 min after the demise of the previous tornado in the same storm, then these tornadoes were counted separately. The approximate time of TC tornadoes were determined by examining the time at which the tornadic vortex signatures were identified in the radial velocity field (if any). Considering that most reports only had a qualitative description of the damage in some parts of the tornado damage area and few damage surveys were performed with the objective of estimating the tornado strength along the whole tornado track, our statistics do not include the strength of TC tornadoes.

3. Statistics for TC tornadoes in China

3.1 TC tornadoes from 2006 to 2018

Figure 1 shows the statistical results for our survey of TC tornadoes in China. A total of 64 TC tornadoes were cataloged for these 13 years, with a mean of five per year. There was an outbreak of TC tornadoes in 2018, which directly increased the annual mean number (Figure 1a). In 2018, TCs Yagi and Mangkhut spawned 11 and five tornadoes, respectively. There was no noticeable trend in the annual occurrence of TC tornadoes. TC tornadoes primarily occurred in August (63%), the month with the maximum number of TCs in the northwest Pacific basin (Figure 1b). The number of tornadoes may be underestimated as a result of the limited visibility at night or a lack of observers at sea or in fields or untraversed mountainous areas. The occurrence of TC tornadoes showed a clear diurnal variation, with a high frequency in the afternoon (Figure 1c); 50% of TC tornadoes occurred between 12:00 and 18:00 BJT.

There were two preferred geographical regions for the occurrence of TC tornadoes: coastal areas in the tropics and coastal areas in the midlatitudes (Figure 2). Guangdong and Jiangsu provinces had the highest occurrences of TC tornadoes, where there are also the most records of traditional tornadoes (i.e., non-TC tornadoes) (Fan and Yu, 2015; Chen et al., 2018). The TC tornadoes mainly occurred in areas with relatively flat topography (Figure 2). About 95% of the TC tornadoes occurred within 250 km of the coastline. Remarkably, 16 tornadoes (25% of the total) occurred in the Pearl River Delta region (Figure 2, inset), where there are large urban agglomerations with large populations. The frequently occurred TC tornadoes, in addition to their parent TCs, are a great threat to human life.

TC tornadoes mainly occurred in the northeast quadrant with respect to the TC center, rather than the right-front quadrant relative to the TC motion. Using Earth-relative coordinates, a large fraction of the tornadoes (72%) occurred in the northeast quadrant of their parent TCs (Figure 3a) with a median azimuthal angle of 35° (Figure 4a). Using TC motion-relative coordinates, however, about 41% of the tornadoes occurred in the right-front quadrant and a similar percentage occurred in the right-rear quadrant (Figure 3b). The median azimuthal angle was approximately 0° (Figure 4a). The distances between the TC center and the corre-

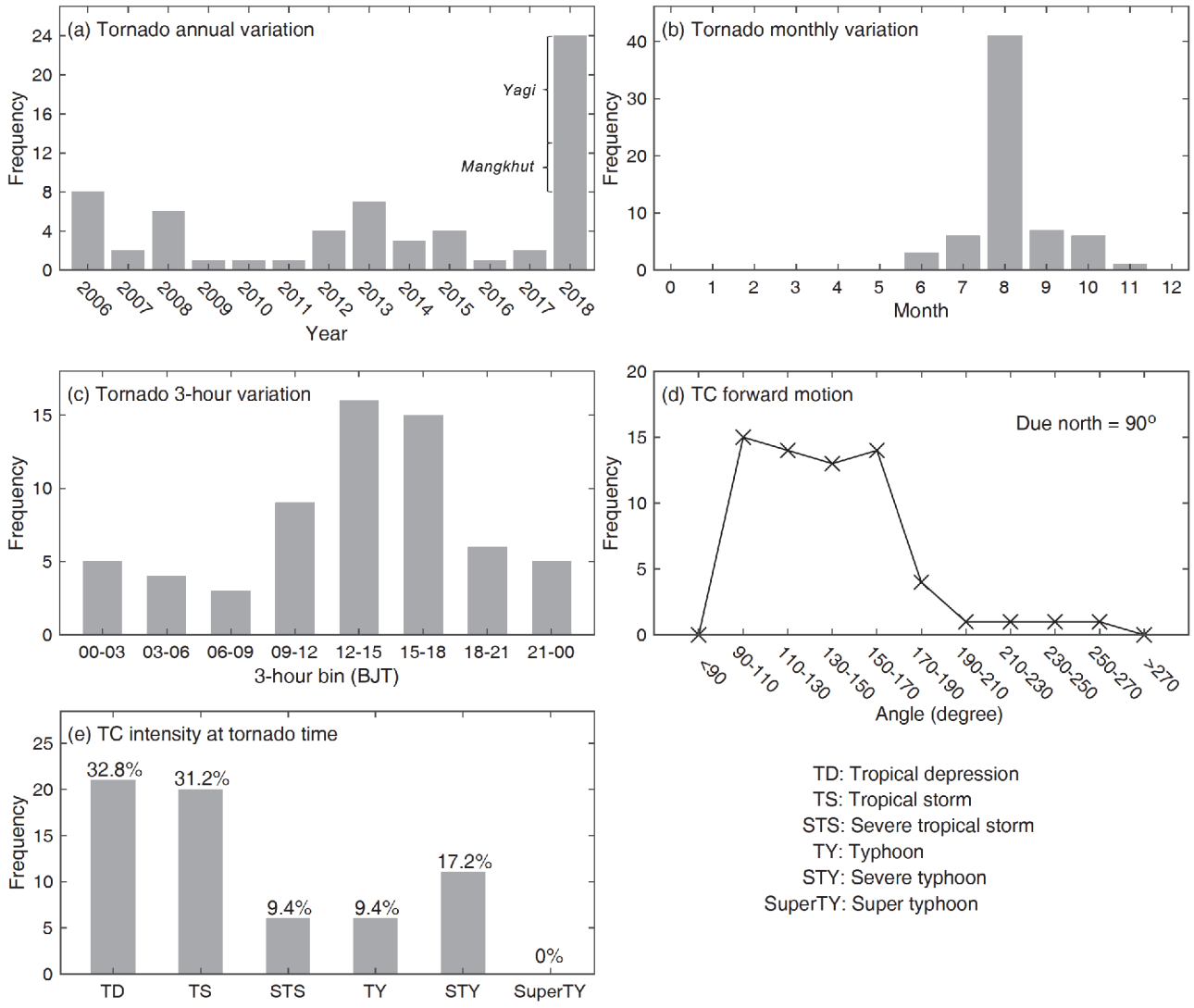

Figure 1 Statistics for TC tornadoes in China from 2006 to 2018, including the variation in the annual (a), monthly (b) and daily (c) occurrence frequency. The forward motion (d) and intensity of the TC (e) at the time of the tornado are also shown.

sponding tornado primarily ranged from 250 to 500 km with a median of 361 km (Figure 4b). About 94% of the TC translational motions were toward the northwest at the time of the tornado (Figure 1d).

The surveyed tornadoes were spawned by 32 TCs, including 30 that made landfall. For reference, 110 TCs landed in China (including the islands of Hainan and Taiwan) during the time period 2006–2018. Some of the data for landfalling TCs were obtained from the website tcdata.typhoon.org.cn (Ying et al., 2014). Therefore about 27% of the TCs that made landfall spawned tornadoes. It is worth noting that tornado-producing TCs are not necessarily TCs that eventually make landfall in China. For example, a non-landfalling TC that only lands in Vietnam may spawn tornadoes in Hainan Province. Two of the 32 tornadic TCs did not make landfall.

The variation in the time of TC tornadoes with respect to the landfall of the TCs was generally identical to that surveyed in the United States (e.g., Novlan and Gray, 1974; Gentry, 1983; Weiss, 1987; McCaul Jr, 1991). About 67% of all the surveyed TC tornadoes occurred after the TC had made landfall. The tornado activity primarily occurred within a period from –12 to 36 h relative to the landfall of the TC, encompassing 63% of the tornadoes (Figure 5a), in contrast with 75% of the tornadoes in the United States (Figure 5b; McCaul Jr, 1991). More specifically, most TC tornadoes in China occurred 12–36 h after landfall, accounting for 36% of the tornadoes. McCaul Jr (1991) reported that most U.S. TC tornadoes (46%) were spawned within 12 h of landfall. Such a difference may partly be attributed to the difference in the orientation of the coastlines between China and the United States. A large number of U.S. TCs make landfall from the Gulf of Mexico, where the northeast quadrant of the TCs covers a larger land area than

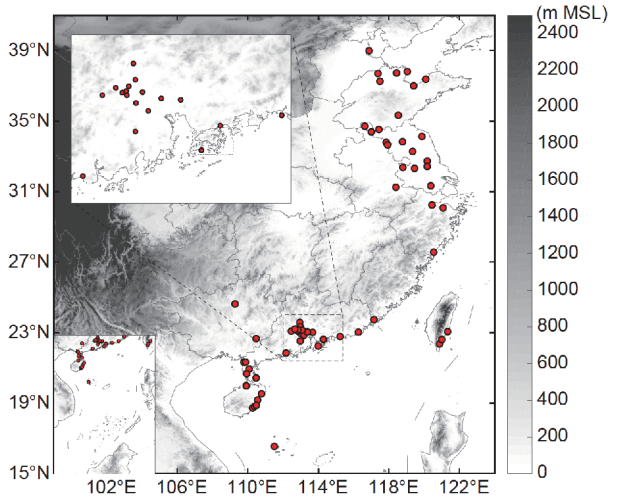

Figure 2 Locations of TC tornadoes (red dots) in China from 2006 to 2018. The region around the Pearl River Delta is enlarged in the upper-left corner. Terrain heights (shaded) are also shown for reference.

that of TCs landing in South or East China. Because most TC tornadoes are produced in the northeast quadrant of their parent TCs, there might be undetected tornadoes at sea when a TC makes landfall in China.

These tornadic TCs produced tornadoes primarily at the intensity of TD (33%) and TS (31%) (Figure 1e). For example, the most tornado-productive TC Yagi (2018), spawned its tornadoes at the intensity of TD (eight tornadoes) and TS (three tornadoes). No TC spawned tornado at the intensity of super typhoon in this study. The surveyed TC tornadoes mainly took place in relatively weak TCs probably partly due to the orientation of coastlines in China. Since TCs generally come from the east, the northeast quadrant (where TC tornadoes tend to be spawned) of a near offshore strong TC is primarily located at sea where there are rare tornado observations. TCs often rapidly weaken shortly after they make landfall and start to produce tornadoes over land in their northeast quadrants.

3.2 TC tornadoes in 2018

TC tornado activity in 2018 was notable in China, contributing 37.5% of the TC tornadoes in the previous 13 years. Eleven TCs landed in China (including the islands of Hainan and Taiwan) and seven spawned at least one tornado. There were 24 reported TC tornadoes, all of which were confirmed by the authors or local meteorological agencies (Table 1). There was direct visual evidence (i.e., videos or photos) for 17 tornadoes. Figure 6 shows some snapshots of the reported tornadoes. Both wedge- and rope-shaped tornadoes were identified. Multiple relatively small-scale vortices were seen to coalesce to form a large wedge tornado (e.g., the tornado on 14 August, Dongying, Shandong).

The first tornado outbreak event in the modern history of China was recorded in 2018 and remains the only recorded outbreak event. According to the *Glossary of Meteorology*, a tornado outbreak event is the occurrence of multiple tornadoes associated with a particular synoptic-scale system (AMS, 2018). An occurrence of ten or more tornadoes is typically defined as a tornado outbreak event (Galway, 1977). TC Yagi (2018) spawned at least 11 tornadoes (magenta dots in Figure 7a) within a 20-h period in central eastern China. Most of these tornadoes occurred one day after rather than on the day of the landfall of the parent TC. This is consistent with the results of McCaul Jr (1991), who showed that, although the largest number of TC tornadoes is generally spawned on the day of landfall, some outbreaks of TC tornadoes have occurred one or two days after the landfall of their parent TC. The total number of tornado

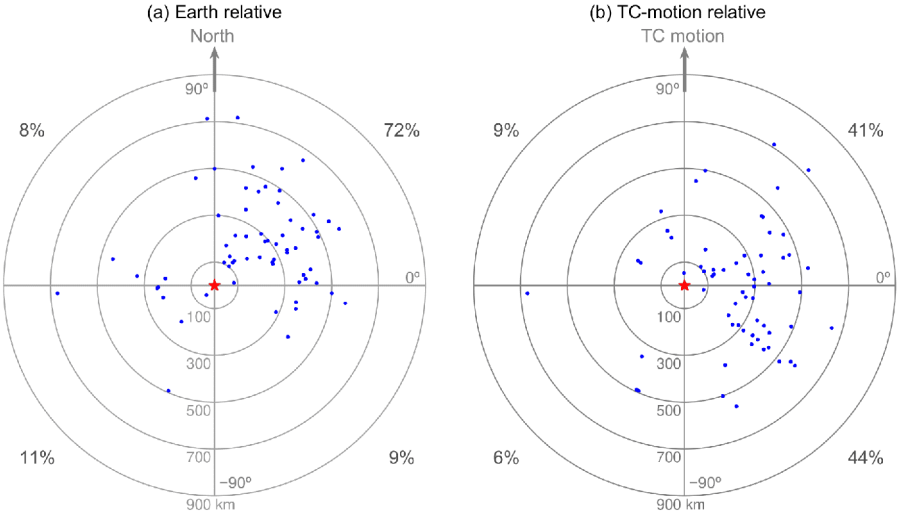

Figure 3 Locations of TC tornadoes (dots) relative to the eye of their parent TC (star) at the time of each tornado in China from 2006 to 2018 shown on Earth-relative (a) and TC motion-relative coordinates (b).

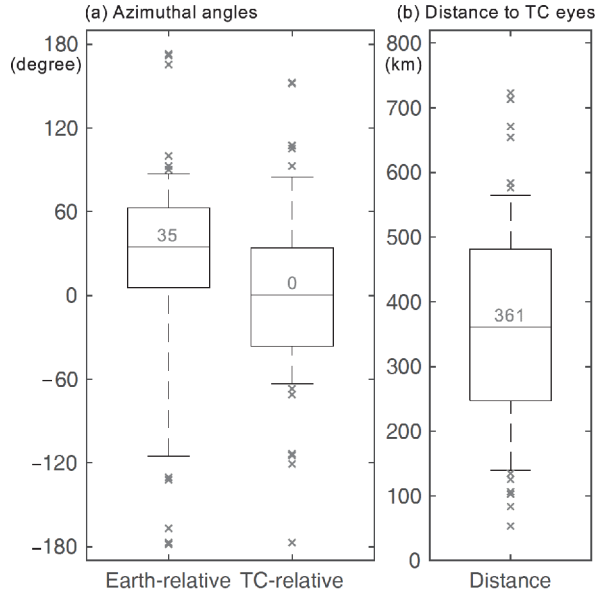

Figure 4 Box-and-whisker diagrams for the azimuthal angles (units: degree) (a) and distances (units: km) (b) of the tornado locations relative to the eyes of their parent TC at the time of each tornado in China from 2006 to 2018. In (a), the due north in the Earth-relative (left) coordinate and the TC forward motion in the TC motion-relative (right) coordinate are 90° as shown in Figure 3. In the box-and-whisker diagrams, the percentile extents and corresponding values represent the 25–75th percentiles for the boxes, the 10–90th percentiles for whiskers and the 50th percentiles for the lines in boxes. Values greater/smaller than the 90th/10th percentile are shown by crosses.

reports for TC Yagi (2018) (or other TCs) is likely to be an underestimate of the true number of tornadoes because of the lack of observers when tornadoes occur at night or offshore.

The Foshan city of Guangdong Province is one of the most tornado-prone areas in China. It was hit by two TC tornadoes in 2018. The first occurred in TC Ewiniar (2018) on the afternoon of 8 June 2018. The other TC tornado was spawned on the morning of 17 September by TC Mangkhut (2018). Fortunately, the Foshan Tornado Research Center, established in 2013, successfully issued tornado warnings prior to both tornadoes. TC Mangkhut (2018) produced another tornado in Zhaoqing city (neighboring Foshan), for which the Foshan Tornado Research Center also issued a successful tornado warning.

4. Key environmental features of TC tornadoes in China

This section presents an analysis of the key environmental conditions that are conducive for the formation of TC tornadoes. We focus on two parameters, the storm relative helicity (SRH) and convective instability with entrainment effects taken into account, which have been shown to be useful for assessing the potential for the production of TC tornadoes (Sueki and Niino, 2016). Due to the fact that a larger bias of TC intensity and size in the analysis/reanalysis data may introduce a larger uncertainty for the distributions of the computed thermodynamic or kinetic variables, a good representation of TC intensity and structure would guarantee the validity of our analysis. In the present study, we used the National Centers for Environmental Prediction (NCEP) Final Operational Global Analysis (NCEP FNL) which has been demonstrated having the best performance in representing the TC intensity and warm-core structure (Gao et al., 2018). The representative environment of a tornado was determined using the NCEP FNL data at the hour closest to the time of the tornado. The composite of an environmental parameter was obtained by simply superposing the TC centers and calculating the average value. Note that the examination of key environmental parameters was not intended to be a search for a "magic bullet" to directly forecast tornadoes in a TC envelope. Rather, the spatial distribution of these parameters relative to the occurrence of TC tornadoes was examined to determine the principal environmental conditions that favor TC tornadogenesis.

4.1 Kinematic environment: SRH

Environments with a large wind shear in the lower tropo-

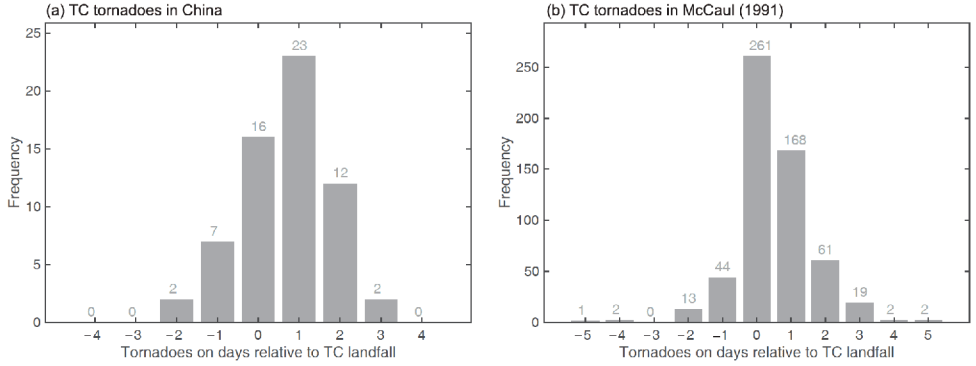

Figure 5 Temporal distribution of TC tornadoes in China from 2006 to 2018 (a) and TC tornadoes in the United States from 1948 to 1986 (b) (adapted from the Figure 15 in McCaul Jr 1991) relative to the day of TC landfall. Day 0 means that the tornado was spawned within 12 h of landfall of the TC and day 1 means that the tornado was spawned from 12 to 36 h after landfall of the TC.

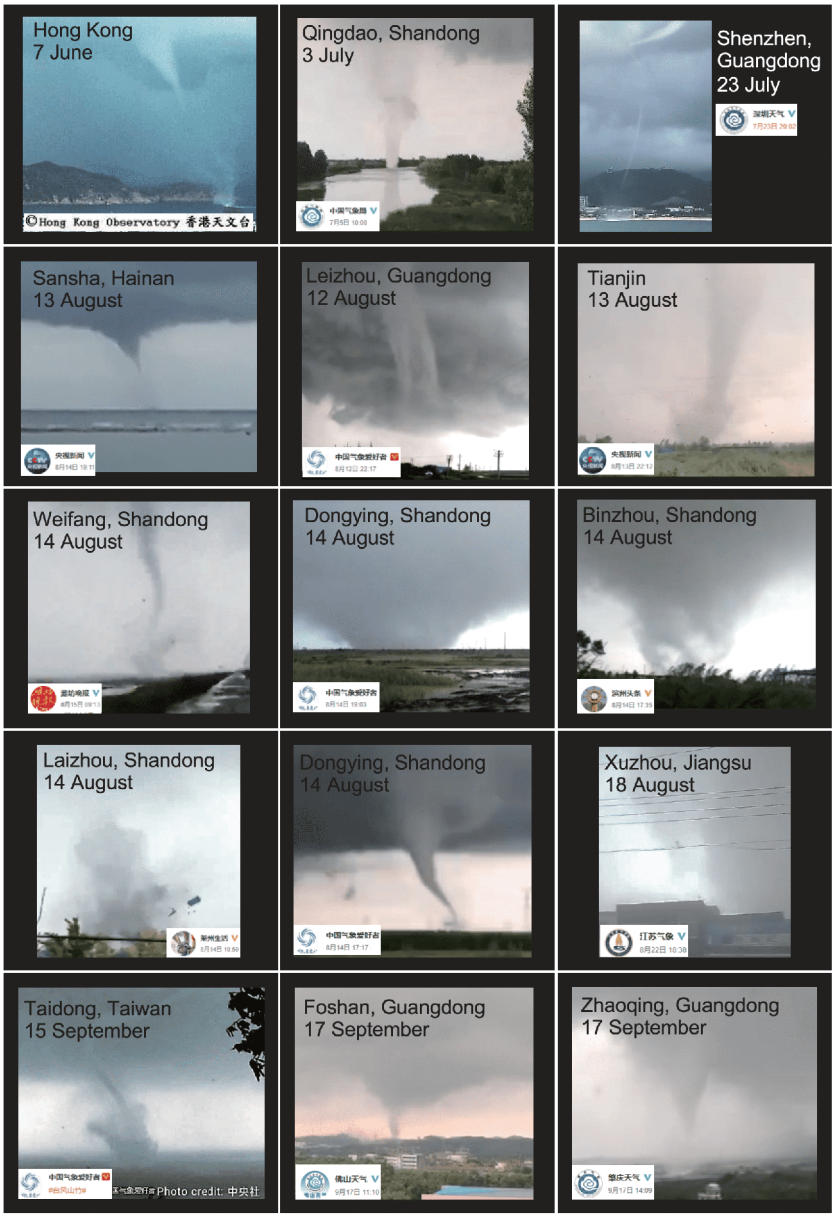

Figure 6 Gallery of the TC tornadoes photographed in China in 2018 and available online at https://weibo.com. The credits for these photographs is indicated in each panel.

sphere have been found to increase the risk of occurrence of TC tornadoes (Novlan and Gray, 1974; McCaul Jr, 1991). In particular, the area of large SRH was shown to be well collocated with the locations of TC tornadoes (e.g., McCaul Jr, 1991; Sueki and Niino, 2016). The SRH is a measure of the potential for cyclonic updraft rotation in right-moving supercells. It can be calculated by integrating the storm-relative streamwise vorticity from the ground to a given altitude (Davies-Jones, 1984):

$$\mathrm{SRH} = \int_0^H (\mathbf{V}_\mathrm{h} - \mathbf{C}) \cdot \left(\mathbf{k} \times \frac{\partial \mathbf{V}_\mathrm{h}}{\partial z} \right) \mathrm{d}z, \quad (1)$$

where H is the given altitude, $\mathbf{V}_\mathrm{h}$ is the horizontal wind, $\mathbf{C}$ is the storm motion and $\mathbf{k}$ is the unit vector in the vertical direction. The SRH obtained from 0 to 1 km above the ground layer (0–1 km SRH) has been found to be a good parameter with which to assess the potential of occurrence of tornadic supercells (Rasmussen, 2003; Thompson et al., 2003, 2007). Based on a 23-year database of TC tornadoes in Japan, Sueki and Niino (2016) showed that the 0–3 km SRH was a good parameter for TC tornadoes. We applied both the 0–1 km and 0–3 km SRH values to diagnose the kinematic environment of the TC tornadoes in China.

The area of large composite 0–1 and 0–3 km SRH generally collocated with the locations of TC tornadoes in China (Figure 8). A slightly better collocation was found in the 0–1 km SRH than in the 0–3 km SRH. Consistent with the results in Sueki and Niino (2016), the composite SRH peaked in the

Table 1 Tropical cyclone tornadoes recorded in China in 2018[a)]

No.	TC	Intensity	Tornado date	Location
1	Ewiniar	TS	7 June	Hong Kong
2	Ewiniar	TS	8 June	Foshan, Guangdong
3	Nameless	TD	23 July	Shenzhen, Guangdong
4	Bebinca	TS	12 August	Leizhou, Guangdong
5	Bebinca	TS	13 August	Sansha, Hainan
6	Yagi	TS	13 August	Tianjin
7	Yagi	TS	13 August	Xuzhou, Jiangsu
8	Yagi	TS	13 August	Suzhou, Anhui
9	Yagi	TD	13 August	Zaozhuang, Shandong
10	Yagi	TD	14 August	Yizheng, Jiangsu
11	Yagi	TD	14 August	Weifang, Shandong
12	Yagi	TD	14 August	Dongying, Shandong
13	Yagi	TD	14 August	Laizhou, Shandong
14	Yagi	TD	14 August	Binzhou, Shandong
15	Yagi	TD	14 August	Dongying, Shandong
16	Yagi	TD	14 August	Dezhou, Shandong
17	Rumbia	TD	18 August	Xuzhou, Jiangsu
18	Rumbia	TD	18 August	Xuzhou, Jiangsu
19	Rumbia	TD	19 August	Linyi, Shandong
20	Mangkhut	STY	15 September	Taidong, Taiwan
21	Mangkhut	STY	15 September	Taidong, Taiwan
22	Mangkhut	STY	16 September	Taidong, Taiwan
23	Mangkhut	TS	17 September	Foshan, Guangdong
24	Mangkhut	TS	17 September	Zhaoqing, Guangdong

a) Nameless means that the tropical cyclone was not given a name because it did not reach the intensity of tropical storm. The date of the tornado is given in Beijing time (BJT=UTC+8 h).

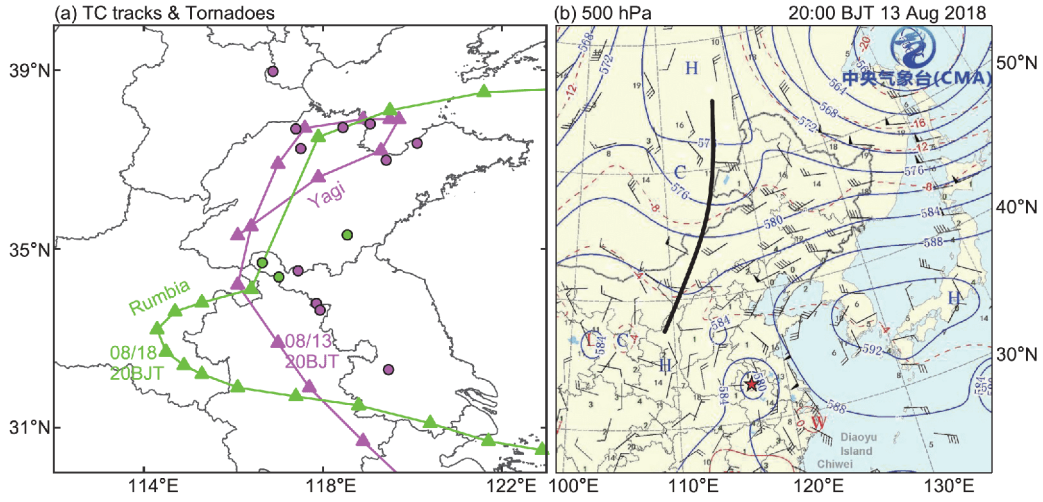

Figure 7 (a) Best tracks of TCs Yagi (magenta) and Rumbia (green) in 2018. The locations of tornado (dots) are shown in the corresponding colors. The TC centers (triangles) are plotted every 6 h. The data for the track of Rumbia were obtained from the National Meteorological Center of China Meteorological Administration (http://typhoon.nmc.cn/web.html). (b) Synoptic chart provided by the China Meteorological Administration with geopotential heights (blue contours; units: dagpm), horizontal winds and temperature (red contours; units: °C) at 500 hPa at 20:00 BJT on 13 August 2018. The half-barb, full-barb and pennant symbols represent wind speeds of 2, 4 and 20 m s^{-1}, respectively. The location of TC Yagi is shown by the red star.

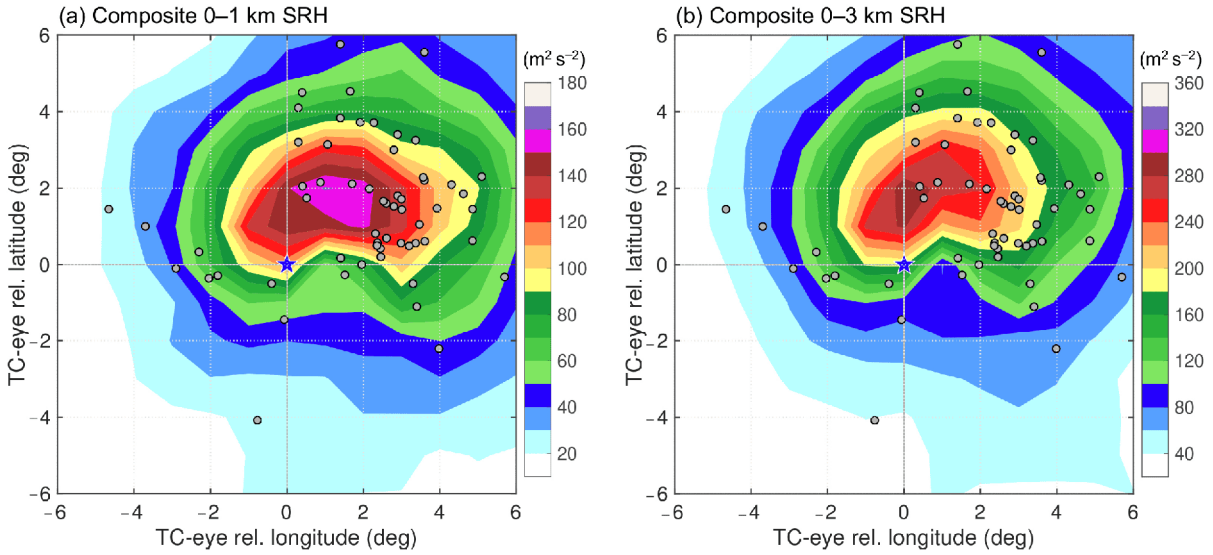

Figure 8 Composite horizontal distributions of the (a) 0–1 km and (b) 0–3 km SRH around the TC eyes (blue stars). The solid gray circles represent the locations of TC tornadoes in 2006–2018 relative to the eye of their parent TC. The X (Y) axis is arranged in the TC eye relative longitude (latitude) for convenience.

northeast quadrant relative to the TC center. Large SRH values were primarily located within about 600 km of the TC center. Around the time of TC tornadoes, the 0–1 km SRH at the location of the TC tornadoes mainly ranged from 75 to 177 $m^2 s^{-2}$ with a median of 103 $m^2 s^{-2}$ (Figure 9a), which is about half the magnitude of the SRH in the United States (Edwards, 2012). The 0–1 km SRH values even exceeded 350 $m^2 s^{-2}$ for some TC tornadoes. Previous studies have suggested that a large low-level SRH favors the production of numerous rotating updrafts, which further favors supercells and tornadoes (Rasmussen, 2003; Thompson et al., 2012; Knupp et al., 2014). These results suggest that the tornado risk was particularly high in terms of kinematic features within about 600 km of the TC center in the northeast quadrant.

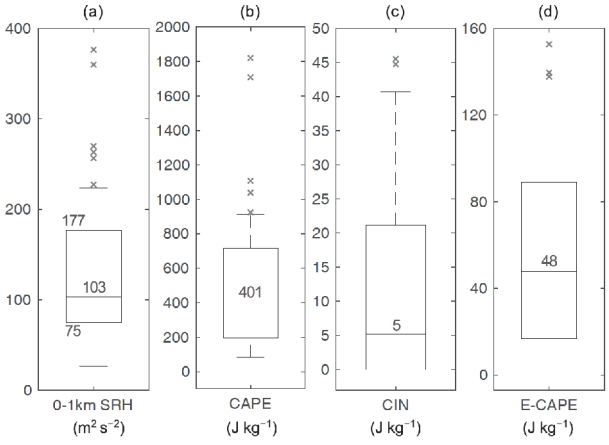

Figure 9 Box-and-whisker diagrams for 0–1 km SRH (a) and mixed layer CAPE (b), CIN (c) and E-CAPE (d) at the locations of TC tornadoes in China in 2006–2018. In the box-and-whisker diagrams, the percentile extents and corresponding values represent the 25–75th percentiles for boxes, the 10–90th percentiles for whiskers and the 50th percentiles for the lines in boxes. Values exceeding the 90th percentile are shown by crosses.

4.2 Thermodynamic environment: convective instability

The area of large convective available potential energy (CAPE) has been long shown to not well collocate with the locations of TC tornadoes (e.g., McCaul Jr, 1991). Many previous studies have emphasized the importance of the entrainment of dry air in the mid-troposphere on the outbreak of TC tornadoes (e.g., Hill et al., 1966; Novlan and Gray, 1974; McCaul Jr, 1987; Curtis, 2004; Eastin and Link, 2009). By considering the effects of entrainment, Sueki and Niino (2016) suggested that the entraining CAPE (E-CAPE) may be a suitable thermodynamic parameter for assessing the potential occurrence of TC tornadoes.

In the parcel theory, CAPE represents the amount of buoyant energy available to accelerate a parcel vertically and is calculated by integrating the buoyancy of a lifted parcel between the level of free convection (LFC) and the equilibrium level (EL):

$$\mathrm{CAPE} = \int_{\mathrm{LFC}}^{\mathrm{EL}} \frac{T_{\mathrm{v}}' - \mathbf{T}_{\mathrm{v}}}{\mathbf{T}_{\mathrm{v}}} \mathrm{g} \mathrm{d}z, \tag{2}$$

where T_{v}' is the virtual temperature of the lifted parcel, $\mathbf{T}_{\mathrm{v}}$ is the ambient virtual temperature and g is the gravitational acceleration. We obtained E-CAPE by updating T_{v}' considering the effects of entrainment using the algorithms of Sueki and Niino (2016), which are based on the Lagrangian

parcel model (Romps and Kuang, 2010). The ascending air parcel was assumed to entrain environmental air at a constant mass entrainment rate (λ). In the present study, all the values of CAPE, E-CAPE and convective inhibition energy (CIN) were calculated using an initial parcel obtained by averaging the relevant variables in the mixed layer from the surface to 1 km above ground level. The area of large composite E-CAPE calculated by air parcels lifted from the surface or the most unstable layer (lowest 300 hPa) were not well collocated with the locations of TC tornadoes.

Figure 10 shows the composite horizontal distribution of CAPE and CIN around the centers of tornado-producing TCs. Similar to the results of Sueki and Niino (2016), most of the tornadoes were located in a region with a moderate CAPE, whereas the area with a large value of CAPE was located to the southeast of the TC center (Figure 10a). The median value of CAPE was 401 J kg^{-1} (Figure 9b), which was comparable with the average CAPE (253 J kg^{-1}) for the TC tornado environment in the United States (McCaul Jr, 1991). Figure 10b shows that the surveyed tornadoes were mainly located in a region with a fairly small CIN with a median of 5 J kg^{-1} (Figure 9c). Compared with other quadrants, it was much easier for the air parcels in the northeast quadrant to overcome the convective barrier and realize buoyant updrafts. As a result, CIN seems to be a better thermodynamic parameter for assessing TC tornadoes than CAPE.

Although the CAPE in the northeast quadrant was not large, this does not mean that the air parcels were characterized by a smaller convective potential than those in other quadrants (e.g., the southeast quadrant). Figure 11 shows the composites of the computed E-CAPE with different entrainment rates. In general, the regions in which TC tornadoes were located were characterized by a large E-CAPE. The E-CAPE values were roughly an order of magnitude smaller than those of CAPE because the lifted parcel entrains unsaturated air in the mid-troposphere and thus the amount of latent heat released per unit mass in the parcel decreases. Sueki and Niino (2016) suggested that a mass entrainment rate of 20% km^{-1} shows the best correspondence between the spatial distribution of TC tornadoes in Japan and that of the composite E-CAPE. In the present study, the area of large E-CAPE with a mass entrainment rate >20% km^{-1} seemed to have a better spatial collocation with the locations of TC tornadoes, especially for λ=40% km^{-1} and λ=50% km^{-1} (Figure 11c, 11d). The following analysis was performed based on E-CAPE with λ=40% km^{-1}. The median E-CAPE for these TC tornadoes was 48 J kg^{-1} (Figure 9d).

4.3 Tornado-productive TC versus tornado-unproductive TC

To investigate whether tornado-productive events can be inferred, we performed an analysis by comparing the environments (e.g., SRH and E-CAPE) between tornado-productive and tornado-unproductive TCs. The selected tornado-productive TC was Yagi (2018), which landed in central eastern China during the evening of 12 August 2018 and spawned 11 tornadoes from 13 to 14 August (Table 1). The selected tornado-unproductive TC was Rumbia (2018), which made landfall during the evening of 16 August 2018 and had a track near that of Yagi (Figure 7a). Rumbia spawned two tornadoes in Xuzhou, Jiangsu Province and one tornado in Linyi, Shandong Province in the early evening of 18 and 19 August, respectively (Table 1).

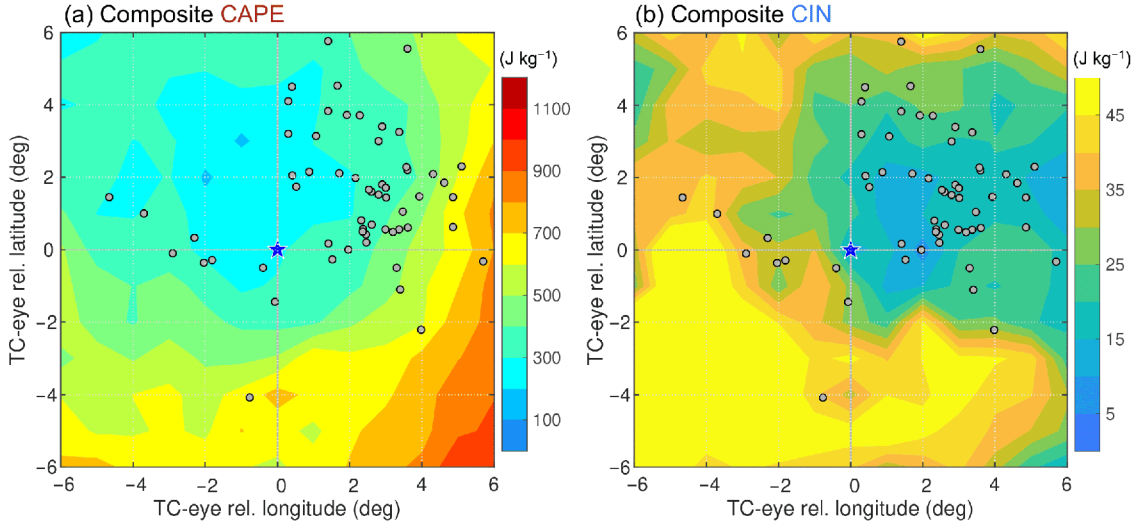

Figure 10 Composite horizontal distributions of the (a) CAPE and (b) CIN around the eyes of the TC (blue stars). The solid gray circles represent the locations of TC tornadoes in 2006–2018 relative to the eye of their parent TC. The $X(Y)$ axis is arranged in the TC eye relative longitude (latitude) for convenience.

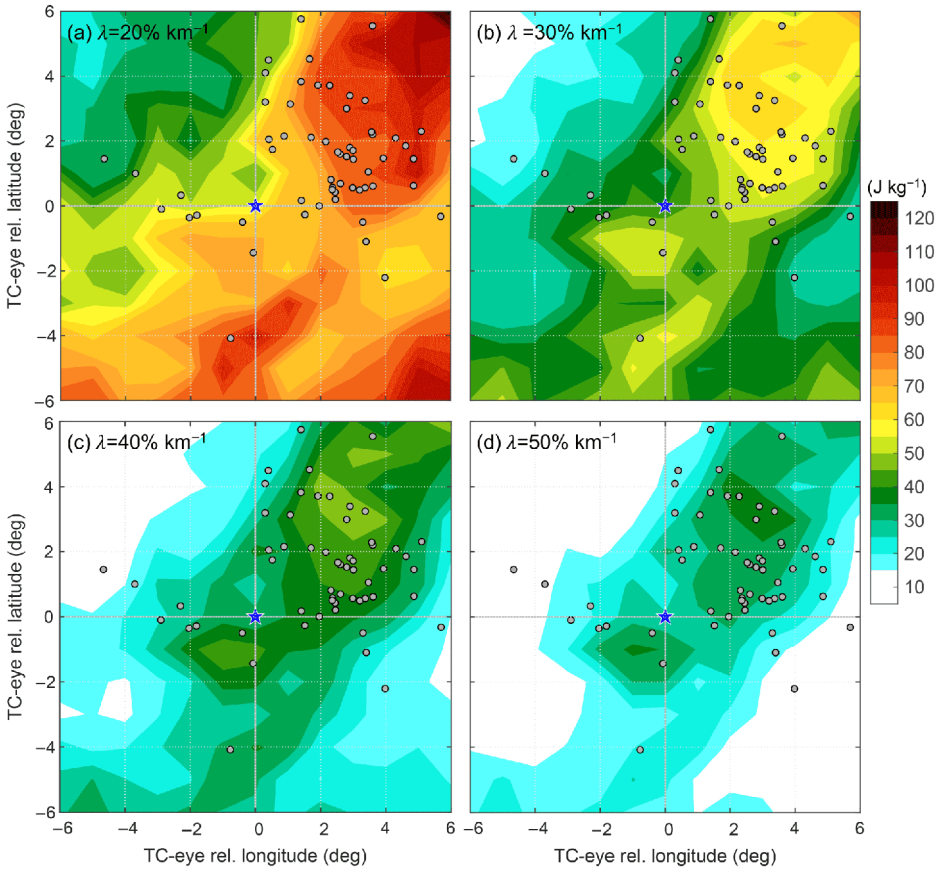

Figure 11 Composite horizontal distributions of the E-CAPE with mass entrainment rates (λ) of 20% (a), 30% (b), 40% (c) and 50% km^{-1} (d). The solid gray circles represent the locations of TC tornadoes in 2006–2018 relative to the eye of their parent TC. The X(Y) axis is arranged in the TC eye relative longitude (latitude) for convenience.

Mixed results were found in the comparison of the thermodynamic and kinematic parameters between Yagi and Rumbia. The composite horizontal distributions of the 0–1 km SRH, E-CAPE, CAPE and CIN values around the time of the tornado are shown in Figure 12. For the tornado-productive TC Yagi (2018), most of the tornadoes were located in a region with favorable kinematic and thermodynamic conditions. Specifically, the environment for the formation of tornadoes in Yagi was characterized by large SRH, E-CAPE and CAPE values and a marginal CIN value (Figure 12a–12d). Yagi featured more favorable thermodynamic conditions. The high-value area of the E-CAPE in Yagi was much greater than that in Rumbia and the magnitude of the CAPE in Yagi was also much greater than that in Rumbia. Although the tornadoes in Rumbia formed in an environment with a generally smaller CAPE and a larger CIN than those in Yagi (Figure 12g, 12h), they were located in a zone with large SRH and E-CAPE values (Figure 12e, 12f). Rumbia even had a larger spatial coverage of high SRH values, indicating a kinematic environment more favorable for tornadic activity than that of Yagi.

Although these results showed that the tornado-productive Yagi had a larger E-CAPE value than the tornado-unproductive Rumbia, it was also found that a larger E-CAPE value might not be the key factor in differentiating tornado-productive and tornado-unproductive TCs. By examining the environmental conditions for all the samples of single-tornado TCs, in which TCs individually spawned only one tornado (a total of 21 TCs), we found that the composite environmental conditions were also characterized by large values of SRH and E-CAPE, a moderate CAPE and a relatively small CIN (Figure 13), similar to those for the tornado-productive Yagi. The magnitude and extent of E-CAPE values was even greater than those of TC Yagi (2018). The northeast quadrant of non-tornadic TCs can also be characterized by large SRH and E-CAPE values, although the values of these two parameters are statistically smaller than those for tornadic TCs (Sueki and Niino, 2016). Tochimoto et al. (2019) suggested that composite indices incorporating the E-CAPE, such as the entraining energy helicity index, are useful for assessing the tornado outbreak potential in the warm sector of extratropical cyclones. Further investigations are required in the application of such composite indices to differentiate tornado-productive and tornado-unproductive TCs.

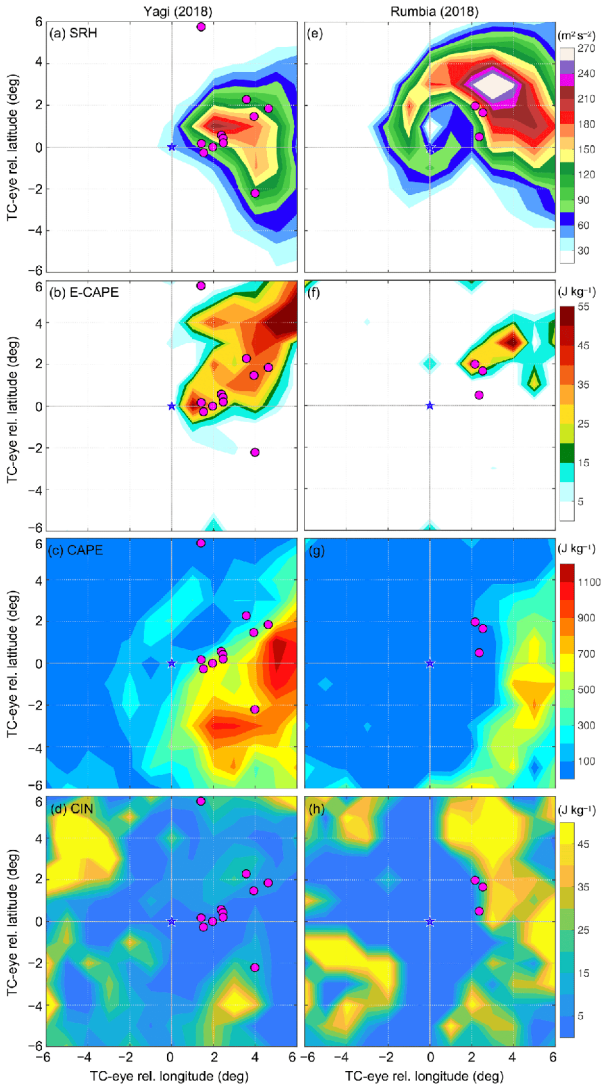

Figure 12 Composite horizontal distributions of the 0–1 km SRH (1st row), E-CAPE (2nd row; mass entrainment rate 40% km^{-1}), CAPE (3rd row) and CIN (4th row) in TCs Yagi (left column) and Rumbia (right column) in 2018. The corresponding TC tornadoes are denoted by magenta dots. The solid gray circles represent the locations of TC tornadoes in 2006–2018 relative to the eye of their parent TC. The $X(Y)$ axis is arranged in the TC eye relative longitude (latitude) for convenience.

Rather than high SRH and E-CAPE values, the intrusions of dry air into the mid-troposphere might be the key contributor to the tornado-productive TC Yagi. It has long been believed that midlevel intrusions of dry air are conducive to the enhancement of deep convection and thus the tornado activity by increasingly destabilizing the atmosphere—for example, due to midlevel evaporative cooling and more insolation in the afternoon boundary layer (Hill et al., 1966; McCaul Jr, 1987; Vescio et al., 1996; Curtis, 2004; Schultz and Cecil, 2009). As seen in the channel 9 water vapor imagery of the Himawari-8 satellite (near 400 hPa; Ma et al., 2017), Yagi was characterized by a distinct reservoir of midlevel dry air in the southeastern sector (Figure 14a). In association with the midlevel southwesterlies, the dry air would be ingested into the storms within the rainbands (Figure 14a, 14b). In fact, the midlevel intrusions of dry air in TC Yagi (2018) were most remarkable on the manual examination of the satellite water vapor imagery for tornadic TCs after July 2015 (when the Himawari-8 data became available). By contrast, the tornadic environment of TC Rumbia (2018) was moist overall (Figure 14c, 14d). In addition to the midlevel dry air intrusions, the occurrence of multiple tornadoes is also likely when a TC interacts with an approaching midlevel trough (e.g., Novlan and Gray, 1974; Verbout et al., 2007; Schultz and Cecil, 2009). Verbout et al. (2007) provided evidence showing that TC tornado outbreaks in the United States were closely associated with approaching midlatitude midlevel troughs which tend to cause the TCs recurve to the northeast quickly. Essentially, such a synoptic situation allows the jet stream to dip equatorward, increasing the deep-layer shear and thus favoring the mesocyclone development and tornadogenesis (Verbout et al., 2007). In the present study, the outbreak of tornadoes was also found to take place when Yagi was interacting with a large-scale midlevel trough and recurving to the northeast (Figure 7b).

5. Summary and discussion

We compiled a 13-year database of tropical cyclone tornadoes (TC tornadoes) in China from 2006 to 2018. Based on this database, we investigated the statistical characteristics of the TC tornadoes, which may help to characterize the tornado threat in landfalling TCs in China.

Our results showed that 27% of the TCs that made landfall were tornadic. We cataloged 64 TC tornadoes, with an average of five per year. TC tornadoes most often occurred in the afternoon and in August. The distribution of TC tornadoes showed two spatial peaks in China, in Jiangsu and Guangdong provinces, which are also the peak regions for traditional tornadoes (i.e., tornadoes not associated with TCs). These TC tornadoes were concentrated in relatively flat regions closer to coastlines than those in the United States (Edwards, 2012). About 95% of the tornadoes occurred within 250 km of the coastline. The distances between the locations of the tornadoes and the centers of their parent TCs ranged from 250 to 500 km. TC tornadoes in China were primarily spawned in the northeast quadrant (Earth-relative coordinates) rather than the right-front quadrant (TC motion-relative coordinates). By contrast, in the United States, both the northeast quadrant and right-front quadrant were favorable locations for TC tornadoes. Differences in the orientation of the coastlines and the translational motion of TCs between China and the United States were the most probable

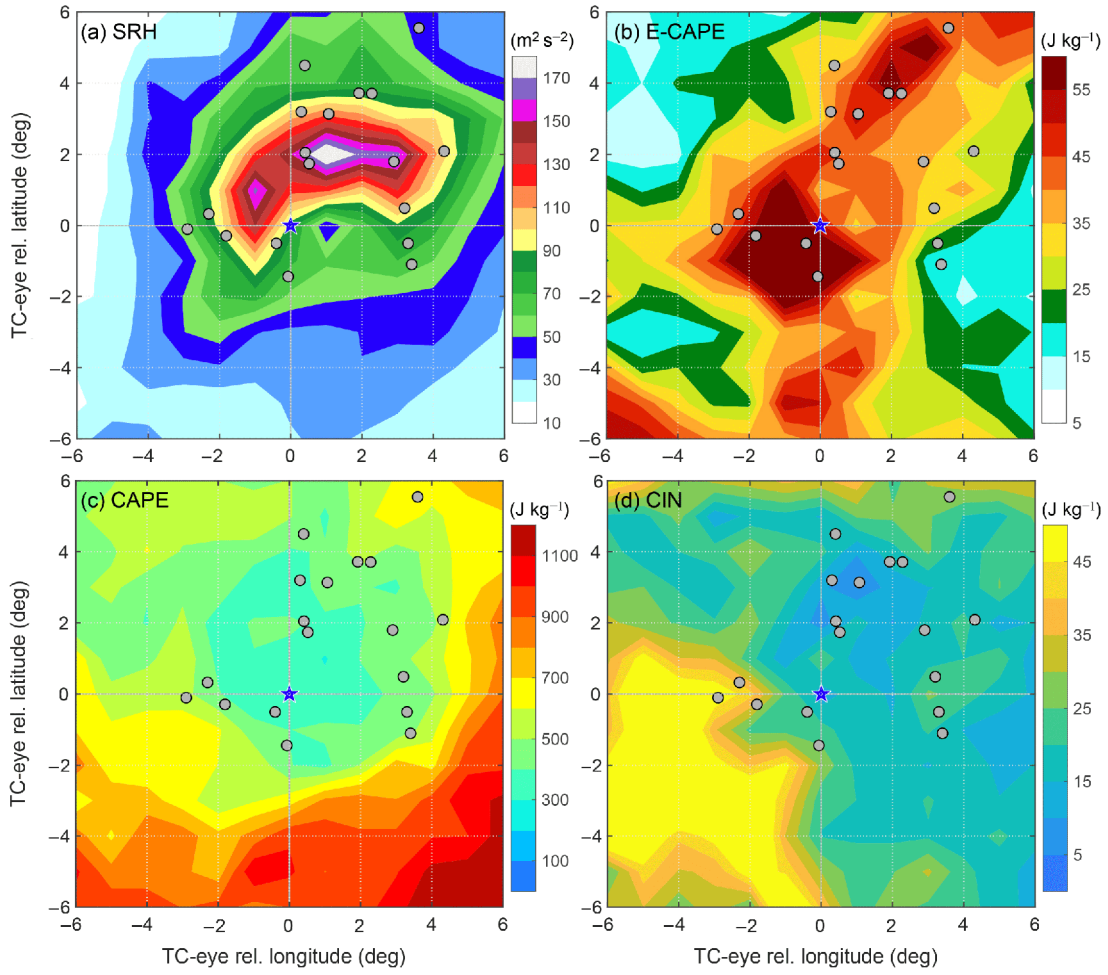

Figure 13 Composite horizontal distributions of the 0–1 km SRH (a), E-CAPE (b) (mass entrainment rate 40% km^{-1}), CAPE (c) and CIN (d) in TCs that spawned only one tornado (21 TC samples during 2006–2018). The solid gray circles represent the locations of TC tornadoes in 2006–2018 relative to the eye of their parent TC. Note that there are three tornadoes located outside of the plotting domain. The $X(Y)$ axis is arranged in the TC eye relative longitude (latitude) for convenience.

cause of such a discrepancy, which requires further investigation. Most of the TC tornadoes in our database were produced in a relatively weak stage of their parent TCs. For example, about 33% of the TC tornadoes formed when their parent TCs had the intensity of tropical depression and about 31% when they had the intensity of tropical storm. Therefore, we can't treat a TC lightly even if it dramatically weakens.

The environmental characteristics of TC tornadogenesis were investigated by examining some key parameters that have been shown to be useful in assessing the potential of TC tornadogenesis. The TC tornadoes tended to be spawned in an environment characterized by large SRH and E-CAPE, consistent with the results for TC tornadoes in Japan (Sueki and Niino, 2016). The statistical value of the 0–1 km SRH at the locations of TC tornadoes was much less than that in the United States.

The year 2018 was unique in terms of TC tornado activity. About 37.5% of the surveyed TC tornadoes occurred in 2018, mainly as a result of the first tornado outbreak event in the modern history of China. This tornado outbreak event occurred one day after TC Yagi (2018) made landfall in central eastern China, in association with significant mid-level intrusions of dry air and the interaction of Yagi with a midlevel trough. However, the location and magnitude of either the SRH or E-CAPE were unable to distinguish tornado-productive and tornado-unproductive TCs, based on a comparison between TC Yagi and Rumbia and single-tornado TCs.

Although we have shown an overall good relationship between the spatial distribution of TC tornadoes and the values of SRH and E-CAPE, we cannot simply use SRH and E-CAPE to forecast TC tornadoes. A TC environment with large values of SRH and E-CAPE does not produce tornadoes most of time. Adequate values of SRH, E-CAPE and CAPE, and a small value of CIN, may only represent favorable atmospheric conditions for a high probability of TC tornadogenesis. Smaller scale processes beyond the en-

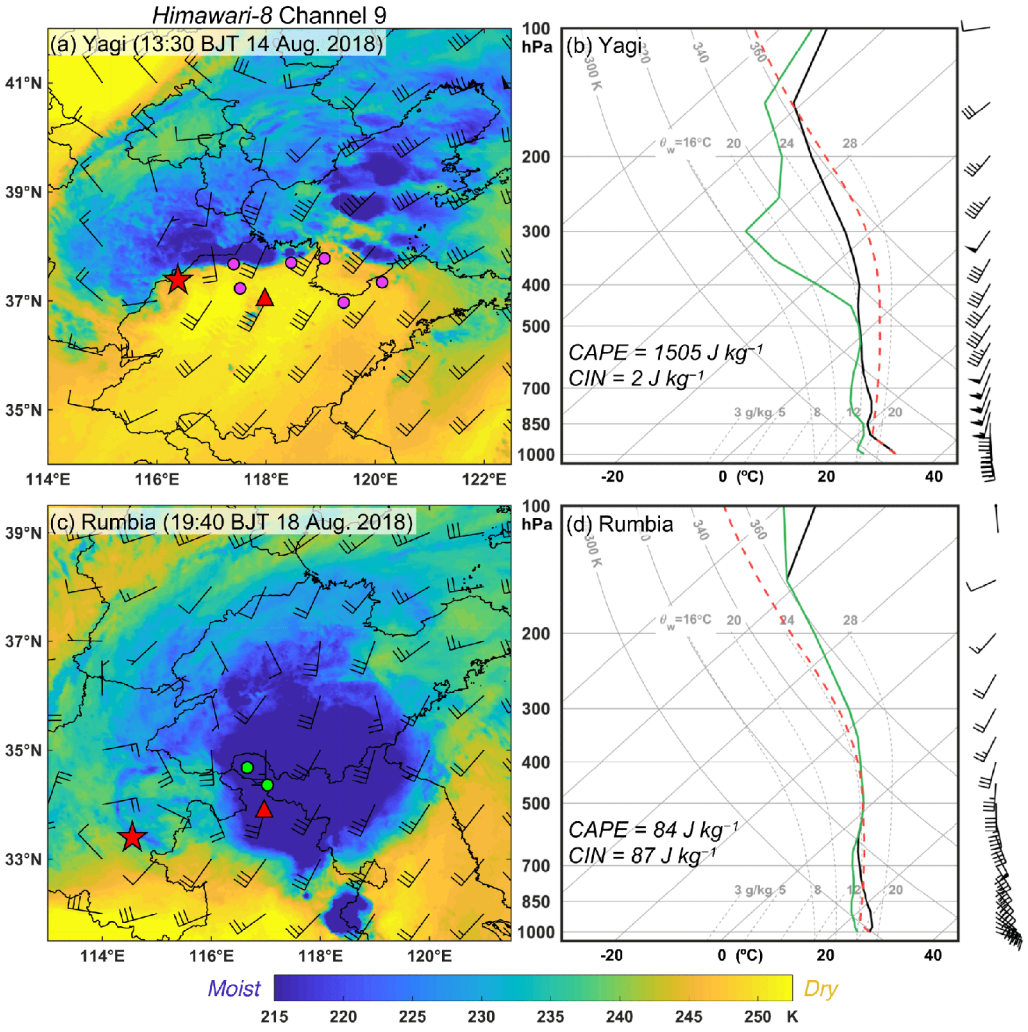

Figure 14 Brightness temperature (units: K) in the channel 9 water vapor imagery of the Himawari-8 satellite (near 400 hPa) at 13:30 BJT on 14 August (a) and 19:40 BJT on 18 August 2018 (c). The horizontal winds at 400 hPa obtained from the NCEP FNL analysis valid at 14:00 BJT on 14 August (a) and 20:00 BJT on 18 August 2018 (c) are shown for reference. The locations of TC are denoted by stars. In (a), tornadoes formed from 10:00 to 13:30 BJT on 14 August 2018 are plotted in magenta. In (b), the two green dots represent the locations of tornadoes that occurred at 18:40 and 19:40 BJT on 18 August 2018, respectively. (b), (d) Skew *T*–log *p* diagrams corresponding to the positions denoted by the triangles in (a) and (c), respectively. The ambient temperature and dewpoint are represented by the black and green curves, respectively. The parcel that ascends undiluted from the surface is shown by the dashed red curve. The half-barb, full-barb and pennant symbols represent wind speeds of 2, 4 and 20 m s^{-1}, respectively.

vironment may eventually determine tornadogenesis within a TC envelope.

Acknowledgements *We thank the numerous people who shared their valuable tornado information (online or privately), including photographs and videos of tornadoes. Special thanks are given to Jiayi Chen from Peking University for providing the tornado database (Chen et al., 2018) and to Zhengzhao Johnny Luo from the City University of New York for helpful comments. We also acknowledge Lijun Yan, Zhaoming Li and Kanglong Cai from the Foshan Tornado Research Center for sharing some of the information on tornadoes. Additional gratitude is extended to the three anonymous reviewers who have greatly aided in the improvement of this work. This work was supported by the National Natural Science Foundation of China (Grant No. 41875051, 41425018 & 41775094), the China Postdoctoral Science Foundation (Grant No. 2019M653146) and the Japan Society for the Promotion of Science KAKENHI (Grant No. JP18H01277).*

References

American Meteorological Society. 2018. Tornado outbreak. Glossary of Meteorology. Available online at http://glossary.ametsoc.org/wiki/Tornado_outbreak

Bai L Q, Meng Z Y, Huang L, Yan L J, Li Z H, Mai X H, Huang Y P, Yao D, Wang X. 2017. An integrated damage, visual, and radar analysis of the 2015 Foshan, Guangdong, EF3 tornado in China produced by the landfalling Typhoon Mujigae (2015). Bull Amer Meteorol Soc, 98: 2619–2640

Barbour G B. 1924. Waterspout and tornado within a typhoon area. Mon Weather Rev, 52: 106–107

Chen J Y, Cai X H, Wang H Y, Kang L, Zhang H S, Song Y, Zhu H, Zheng W, Li F J. 2018. Tornado climatology of China. Int J Climatol, 38: 2478–2489

Chen L S, Ding Y H. 1979. An Introduction to the Western Pacific Typhoon (in Chinese). Beijing: Science Press. 491

Curtis L. 2004. Midlevel dry intrusions as a factor in tornado outbreaks associated with landfalling tropical cyclones from the Atlantic and Gulf

of Mexico. Weather Forecast, 19: 411–427
Davies-Jones R. 1984. Streamwise vorticity: The origin of updraft rotation in supercell storms. J Atmos Sci, 41: 2991–3006
Eastin M D, Link M C. 2009. Miniature supercells in an offshore outer rainband of Hurricane Ivan (2004). Mon Weather Rev, 137: 2081–2104
Edwards R. 2012. Tropical cyclone tornadoes: A review of knowledge in research and prediction. Electronic J Severe Storms Meteorol, 7: 1–61
Fan W J, Yu X D. 2015. Characteristics of spatial-temporal distribution of tornadoes in China (in Chinese). Meteorol Mon, 41: 793–805
Galway J G. 1977. Some climatological aspects of tornado outbreaks. Mon Weather Rev, 105: 477–484
Gao S, Wang D L, Hong H X, Wu N G, Li T. 2018. Evaluation of warm-core structure in reanalysis and satellite data sets using HS3 dropsonde observations: A case study of Hurricane Edouard (2014). J Geophys Res-Atmos, 123: 6713–6731
Gentry R C. 1983. Genesis of tornadoes associated with hurricanes. Mon Weather Rev, 111: 1793–1805
Hill E L, Malkin W, Schulz Jr W A. 1966. Tornadoes associated with cyclones of tropical origin-practical features. J Appl Meteorol, 5: 745–763
Huang X X, Yan L J, Wang S F, Cheng Z Q. 2014. Analysis of the characteristics of tornados in Foshan city and their circulation background (in Chinese). Guangdong Meteorol, 36: 20–24
Knupp K R, Murphy T A, Coleman T A, Wade R A, Mullins S A, Schultz C J, Schultz E V, Carey L, Sherrer A, McCaul Jr. E W, Carcione B, Latimer S, Kula A, Laws K, Marsh P T, Klockow K. 2014. Meteorological overview of the devastating 27 April 2011 tornado outbreak. Bull Amer Meteorol Soc, 95: 1041–1062
Lyons S W. 2004. U.S. Tropical cyclone landfall variability: 1950–2002. Weather Forecast, 19: 473–480
Ma Z Z, Maddy E S, Zhang B L, Zhu T, Boukabara S A. 2017. Impact Assessment of *Himawari-8* AHI Data Assimilation in NCEP GDAS/GFS with GSI. J Atmos Ocean Technol, 34: 797–815
McCaul Jr E W. 1987. Observations of the Hurricane "Danny" tornado outbreak of 16 August 1985. Mon Weather Rev, 115: 1206–1223
McCaul Jr E W. 1991. Buoyancy and shear characteristics of hurricane-tornado environments. Mon Weather Rev, 119: 1954–1978
Meng Z Y, Yan D C, Zhang Y J. 2013. General features of squall lines in East China. Mon Weather Rev, 141: 1629–1647
Meng Z Y, Bai L Q, Zhang M R, Wu Z F, Li Z H, Pu M J, Zheng Y G, Wang X H, Yao D, Xue M, Zhao K, Li Z M, Peng S Q, Li L Y. 2018. The deadliest tornado (EF4) in the past 40 years in China. Weather Forecast, 33: 693–713
Mitsuta Y. 1983. Studies on wind disasters caused by tatsumaki (tornadoes and waterspouts) and severe local storms in Japan (in Japanese with English abstract). Final Report of the Special Research Project for Natural Disaster Sponsored by the Ministry of Education. 124
Niino H, Fujitani T, Watanabe N. 1997. A statistical study of tornadoes and waterspouts in Japan from 1961 to 1993. J Clim, 10: 1730–1752
Novlan D J, Gray W M. 1974. Hurricane-spawned tornadoes. Mon Weather Rev, 102: 476–488
Rasmussen E N. 2003. Refined supercell and tornado forecast parameters. Weather Forecast, 18: 530–535
Romps D M, Kuang Z. 2010. Do undiluted convective plumes exist in the upper tropical troposphere? J Atmos Sci, 67: 468–484
Schultz L A, Cecil D J. 2009. Tropical cyclone tornadoes, 1950–2007. Mon Weather Rev, 137: 3471–3484
Shen S. 1990. A preliminary analysis of the general characteristics and formation conditions of tornadoes ahead of typhoons. Meteorol Mon, 16: 11–16
Spratt S M, Sharp D W, Welsh P, Sandrik A, Alsheimer F, Paxton C. 1997. A WSR-88D assessment of tropical cyclone outer rainband tornadoes. Weather Forecast, 12: 479–501
Sueki K, Niino H. 2016. Toward better assessment of tornado potential in typhoons: Significance of considering entrainment effects for CAPE. Geophys Res Lett, 43: 12597–12604
Suzuki O, Niino H, Ohno H, Nirasawa H. 2000. Tornado-producing mini supercells associated with Typhoon 9019. Mon Weather Rev, 128: 1868–1882
Thompson R L, Edwards R, Hart J A, Elmore K L, Markowski P M. 2003. Close proximity soundings within supercell environments obtained from the Rapid Update Cycle. Weather Forecast, 18: 1243–1261
Thompson R L, Mead C M, Edwards R. 2007. Effective storm-relative helicity and bulk shear in supercell thunderstorm environments. Weather Forecast, 22: 102–115
Thompson R L, Smith B T, Grams J S, Dean A R, Broyles C. 2012. Convective modes for significant severe thunderstorms in the contiguous United States. Part II: Supercell and QLCS tornado environments. Weather Forecast, 27: 1136–1154
Tochimoto E, Sueki K, Niino H. 2019. Entraining CAPE for better assessment of tornado outbreak potential in the warm sector of extratropical cyclones. Mon Weather Rev, 147: 913–930
Verbout S M, Schultz D M, Leslie L M, Brooks H E, Karoly D J, Elmore K L. 2007. Tornado outbreaks associated with landfalling hurricanes in the North Atlantic Basin: 1954–2004. Meteorol Atmos Phys, 97: 255–271
Vescio M D, Weiss S J, Ostby F P. 1996. Tornadoes associated with Tropical Storm Beryl. Miami: 21st Conf on Hurricanes and Tropical Meteorology. 469–471
Weiss S J. 1987. Some climatological aspects of forecasting tornadoes associated with tropical cyclones. Miami: 17th Conf on Hurricanes and Tropical Meteor. 160–163
Yao D, Liang X D, Meng Q, Li J, Wu C, Xie Z S, Chen D D, Guo J P. 2019. Importance of identifying tropical cyclone tornadoes in typhoon warning and defense systems. Chin Sci Bull, 64: 143–145
Ying M, Zhang W, Yu H, Lu X Q, Feng J X, Fan Y X, Zhu Y T, Chen D Q. 2014. An overview of the China Meteorological Administration tropical cyclone database. J Atmos Ocean Technol, 31: 287–301
Zhao K, Wang M J, Xue M, Fu P L, Yang Z L, Chen X M, Zhang Y, Lee W C, Zhang F Q, Lin Q, Li Z H. 2017. Doppler radar analysis of a tornadic miniature supercell during the landfall of Typhoon Mujigae (2015) in South China. Bull Amer Meteorol Soc, 98: 1821–1831
Zheng Y, Yu X D, Ren F M, Cai Q B. 2017. Analysis on a severe tornado process in Hainan triggered by supercell (in Chinese). Meteorol Mon, 43: 675–685
Zheng Y Y, Zhang B, Wang X H, Sun K Y, Mu R Q, Xia W M. 2015. Analysis of typhoon-tornado weather background and radar echo structure (in Chinese). Meteorol Mon, 41: 942–952

(Responsible editor: Dehai LUO)